ISSN 1674-1056
http://cpb.iphy.ac.cn
http://iopscience.iop.org/cpb
中国物理 B
Chinese Physics
中国物理 Chinese Physics B

Linear optical approach to supersymmetric dynamics

Yong-Tao Zhan(詹颙涛)[1,2], Xiao-Ye Xu(许小冶)[1,2], Qin-Qin Wang(王琴琴)[1,2], Wei-Wei Pan(潘维韦)[1,2], Munsif Jan[1,2], Fu-Ming Chang(常弗鸣)[1,2], Kai Sun(孙凯)[1,2], Jin-Shi Xu(许金时)[1,2], Yong-Jian Han(韩永建)[1,2], Chuan-Feng Li(李传锋)[1,2], Guang-Can Guo(郭光灿)[1,2]

Citation: Chin. Phys. B . 2020, 29(1): 014209 . **doi:** 10.1088/1674-1056/ab5efe
Journal homepage: http://cpb.iphy.ac.cn; http://iopscience.iop.org/cpb

What follows is a list of articles you may be interested in

Numerical investigation on coherent mid-infrared supercontinuum generation in chalcogenide PCFs with near-zero flattened all-normal dispersion profiles

Jie Han(韩杰), Sheng-Dong Chang(常圣东), Yan-Jia Lyu(吕彦佳), Yong Liu(刘永)
Chin. Phys. B . 2019, 28(10): 104204 . **doi:** 10.1088/1674-1056/ab3f25

Enhancement and control of the Goos-Hänchen shift bynonlinear surface plasmon resonance in graphene

Qi You(游琪), Leyong Jiang(蒋乐勇), Xiaoyu Dai(戴小玉), Yuanjiang Xiang(项元江)
Chin. Phys. B . 2018, 27(9): 094211 . **doi:** 10.1088/1674-1056/27/9/094211

Research progress of third-order optical nonlinearity of chalcogenide glasses

Xiao-Yu Zhang(张潇予), Fei-Fei Chen(陈飞飞), Xiang-Hua Zhang(章向华), Wei Ji(季伟)
Chin. Phys. B . 2018, 27(8): 084208 . **doi:** 10.1088/1674-1056/27/8/084208

Nonlinear spectral cleaning effect in cross-polarized wave generation

Linpeng Yu(於林鹏), Yi Xu(许毅), Fenxiang Wu(吴分翔), Xiaojun Yang(杨晓骏), Zongxin Zhang(张宗昕), Yuanfeng Wu(吴圆峰), Yuxin Leng(冷雨欣), Zhizhan Xu(徐至展)
Chin. Phys. B . 2018, 27(5): 054214 . **doi:** 10.1088/1674-1056/27/5/054214

Modulation and mechanism of ultrafast transient spectroscopy based on dimethylamino-carbaldehyde derivatives

Tong-xing Jin(金桐兴), Jun-yi Yang(杨俊义), Yu Fang(方宇), Yan-bing Han(韩艳兵), Ying-lin Song(宋瑛林)
Chin. Phys. B . 2018, 27(5): 054208 . **doi:** 10.1088/1674-1056/27/5/054208

Linear optical approach to supersymmetric dynamics*

Yong-Tao Zhan(詹颙涛)[1,2], Xiao-Ye Xu(许小冶)[1,2,†], Qin-Qin Wang(王琴琴)[1,2], Wei-Wei Pan(潘维韦)[1,2], Munsif Jan[1,2], Fu-Ming Chang(常弗鸣)[1,2], Kai Sun(孙凯)[1,2], Jin-Shi Xu(许金时)[1,2], Yong-Jian Han(韩永建)[1,2,‡], Chuan-Feng Li(李传锋)[1,2,§], and Guang-Can Guo(郭光灿)[1,2]

[1] *CAS Key Laboratory of Quantum Information, University of Science and Technology of China, Hefei* 230026, *China*

[2] *Synergetic Innovation Center of Quantum Information and Quantum Physics, University of Science and Technology of China, Hefei* 230026, *China*

(Received 14 August 2019; revised manuscript received 14 October 2019; accepted manuscript online 5 December 2019)

The concept of supersymmetry developed in particle physics has been applied to various fields of modern physics. In quantum mechanics, the supersymmetric systems refer to the systems involving two supersymmetric partner Hamiltonians, whose energy levels are degeneracy except one of the systems has an extra ground state possibly, and the eigenstates of the partner systems can be mapped onto each other. Recently, an interferometric scheme has been proposed to show this relationship in ultracold atoms [*Phys. Rev. A* **96** 043624 (2017)]. Here this approach is generalized to linear optics for observing the supersymmetric dynamics with photons. The time evolution operator is simulated approximately via Suzuki–Trotter expansion with considering the realization of the kinetic and potential terms separately. The former is realized through the diffraction nature of light and the later is implemented using a phase plate. Additionally, we propose an interferometric approach which can be implemented perfectly using an amplitude alternator to realize the non-unitary operator. The numerical results show that our scheme is universal and can be realized with current technologies.

Keywords: linear optics, supersymmetry, quantum simulation

PACS: 42.50.–p, 03.67.–a, 11.30.Pb **DOI:** 10.1088/1674-1056/ab5efe

1. Introduction

In particle physics, to overcome the deficiencies in explaining the dark matter (energy) and the hierarchy problem via the standard model, theoretical physicists developed a concept called supersymmetry (SUSY).[1] Although SUSY can unify the weak, strong, and electromagnetic couplings at high energy and give birth to the dark matter (energy), the existence of SUSY is still controversial due to lack of experimental proof.[2–5] However, with the theoretical developments for nearly half a century, its conceptual structure has provided powerful mathematical tools (SUSY algebras), which have been applied to various fields apart from the high energy physics.[6] One of such fields is the supersymmetric quantum mechanics,[7–10] which involves two supersymmetric partner Hamiltonians. This is a critical concept in SUSY, which originally describes the symmetry between the two basic particles fermions and bosons.[11] By using this concept, a wide range of physical problems can be tackled out, e.g., the physics in stochastic dynamics[12] and in the condensed matter,[13] new technologies can be developed in other subjects, for example, the supersymmetric transformation optics.[14–16]

Supersymmetric quantum mechanics establishes a relation between two partner Hamiltonians. Suppose one of the Hamiltonians $H^{(1)}$ can be factorized as $H^{(1)} = \hat{B}\hat{B}^{\dagger}$, where $\hat{B}^{\dagger}$ denotes the Hermitian conjugate of $\hat{B}$, its supersymmetric partner can then be defined as $H^{(2)} = \hat{B}^{\dagger}\hat{B}$. We can easily find that the eigenenergies of the two systems with Hamiltonians given by $H^{(1)}$ and $H^{(2)}$ are the same (except for the ground state of one Hamiltonian possibly), and their eigenstates can be mapped onto each other through operators $\hat{B}^{\dagger}$ and $\hat{B}$. This relationship is a direct consequence of the supersymmetric algebra, which is independent of the concerned subjects and can be directly applied to other fields.

Recently, Lahrz *et al.* proposed a scheme for implementing the supersymmetric dynamics in ultracold atom systems.[17] In their scheme, they considered verifying the translated version of the supersymmetric relationship between two partner Hamiltonians

$$\hat{B}^{\dagger}\hat{U}^{(1)}(t) = \hat{U}^{(2)}(t)\hat{B}^{\dagger}, \tag{1}$$

where $\hat{U}^{(i)}(t)$ $(i \in \{1,2\})$ is the time evolution operator of the Hamiltonian $H^{(i)}$. The statement of Eq. (1) holds for any time t and is independent of the system's initial state. It was suggested to detect the SUSY via a Mach–Zehnder interference

*Project supported by the National Key Research and Development Program of China (Grant Nos. 2017YFA0304100 and 2016YFA0302700), the National Natural Science Foundation of China (Grant Nos. 11474267, 61327901, 11774335, and 61322506), Key Research Program of Frontier Sciences, Chinese Academy of Sciences (Grant No. QYZDY-SSW-SLH003), the Fundamental Research Funds for the Central Universities of China (Grant No. WK2470000026), the National Postdoctoral Program for Innovative Talents, China (Grant No. BX201600146), China Postdoctoral Science Foundation (Grant No. 2017M612073), and Anhui Initiative in Quantum Information Technologies, China (Grant No. AHY060300).

†Corresponding author. E-mail: xuxiaoye@ustc.edu.cn

‡Corresponding author. E-mail: smhan@ustc.edu.cn

§Corresponding author. E-mail: cfli@ustc.edu.cn

© 2020 Chinese Physical Society and IOP Publishing Ltd

experiment. As shown in Fig. 1, the system is initialized in state ψ_i and then split to evolve along two paths corresponding to the supersymmetric partner Hamiltonians. If equation (1) holds, a constructive interference is supposed to be observed for arbitrary evolution time t.

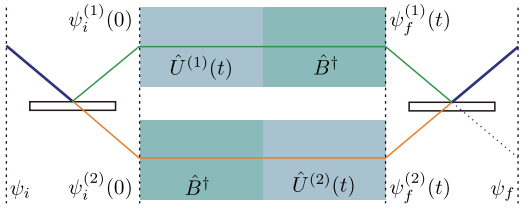


Fig. 1. Interferometric approach to implement the supersysmmetric dynamics.[17] The system, which is initialized in ψ_i, is split into two parts: one evolves according to the time evolution $\hat{U}^{(1)}(t)$ firstly and thereafter an operator $\hat{B}^\dagger$ (green line); the other is diametrically opposite (the orange line). It is supposed that, if the two Hamiltonians governing the evolution of the two parts are superpartner, the final states $\psi_f^{(1)}(t)$ and $\psi_f^{(2)}(t)$ are equal and a constructive interference should be observed after the second beam splitter.

In their scheme, the potential is restricted to a specific form, as a result, the time evolution operator $\hat{U}^{(i)}(t)$ can be realized easily in an ultracold atom system. Their approach in realizing the operator $\hat{B}^\dagger$ (non-unitary) is actually $(\hat{B}+\hat{B}^\dagger)$ which can be approximated with a unitary operator. Although the first $\hat{B}^\dagger$ can be implemented perfectly via setting the initial state to be a ground state, the fidelity of the second $\hat{B}^\dagger$ operation can only reach $1/\sqrt{2}$. While the authors argued that their scheme for implementing the supersymmetric dynamics is experimentally achievable in an ultracold atom system with current technology, this method has never been subjected to an experimental test, probably for the exceedingly high demands upon the fidelity of the initial state as well as the interference visibility. However, these disadvantages can be easily fixed in linear optics.

In this article, we propose to extend their scheme in implementing and detecting the supersymmetric relation (Eq. (1)) into linear optics. We consider to implement the unitary time evolution operator $\hat{U}^{(i)}(t)$ and the non-unitary operator $B^\dagger$ with currently available optical elements. Our scheme overcomes the above difficulties. First, the system can be initialized in an arbitrary state via the spatial light modulator (SLM) and the potential can be set to an arbitrary form by modifying the phase plates. Second, we present a direct approach to implement $\hat{B}^\dagger$ with a Mach–Zehnder interferometer, which can simulate the $\hat{B}^\dagger$ operation with high fidelity.

The article is organized as follows. In Section 2, we show how to implement operators $\hat{U}^{(i)}(t)$ and $\hat{B}^\dagger$ in linear optics, which are two main problems in experimentally implementing supersymmetric dynamics. In Section 3, we set the initial state and potential to a specific form and numerically simulate the process of experiment. In addition, we analyze the precision of our realization. Finally, we present our conclusion in Section 4.

2. Implementing the time evolution operator in linear optics

2.1. Suzuki–Trotter expansion of the time evolution operator

Generally, the Hamiltonian of an isolated system contains two terms, i.e., kinetic energy $\mathcal{P}$ and potential energy $\mathcal{V}$; and the time evolution is described by the Schrödinger equation. However, solving such a differential equation is usually not an easy task even for a simple form of potential. For a time-independent scenario, the time evolution operator is in the form $\hat{U}(t)=\exp[-\mathrm{i}(\mathcal{P}+\mathcal{V})t]$, which is also hard to solve for the noncommutative feature of the two terms. Analog quantum simulation[18,19] of this time evolution needs to construct a controllable system with the same form of the Hamiltonian, which also faces challenges in the experiment.

To date, a variety of approximate formulas have been developed for calculating the time evolution operator.[20–22] The leading one is the Suzuki–Trotter expansion, also called the exponential product formula.[23] To the first and second orders, it respectively reads

$$\mathrm{e}^{t(\hat{A}+\hat{B})}=\lim_{n\to\infty}(\mathrm{e}^{\hat{A}\Delta t}\mathrm{e}^{\hat{B}\Delta t})^n, \tag{2}$$

$$\mathrm{e}^{t(\hat{A}+\hat{B})}=\lim_{n\to\infty}(\mathrm{e}^{\hat{A}\Delta t/2}\mathrm{e}^{\hat{B}\Delta t}\mathrm{e}^{\hat{A}\Delta t/2})^n, \tag{3}$$

where $\hat{A}$ and $\hat{B}$ are arbitrary operators with $t=n\Delta t$. By applying the formula of the second order expansion (Eq. (3)) to our scenario, we can decompose the time evolution operator $\hat{U}(t)$ into two terms, one only contains the kinetic term with the other only containing the potential term, which reads

$$\hat{U}(t)=\lim_{n\to\infty}(\mathrm{e}^{-\mathrm{i}\mathcal{P}\Delta t/2}\mathrm{e}^{-\mathrm{i}\mathcal{V}\Delta t}\mathrm{e}^{-\mathrm{i}\mathcal{P}\Delta t/2})^n. \tag{4}$$

Instead of building a quantum simulation apparatus whose Hamiltonian is in the same form of our concerns, we reach the time evolution operator $\hat{U}(t)$ approximately following Eq. (4).

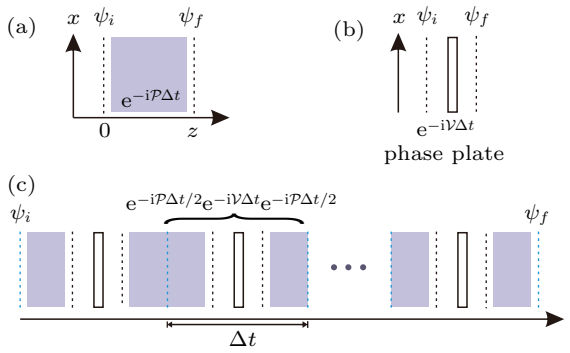


Fig. 2. Implementation of time evolution operator. Panel (a) depicts the diffraction of light in free space (shadow) as the simulation of the propagator of free particle. Panel (b) shows a phase plate (rectangle) acting as a time evolution operator of a delta-kick potential. In (c), combination of (a) and (b) can realize a general time evolution operator for any time scale via the approximation of Suzuki–Trotter expansion (second order).

The kinetic and potential terms in a single step of the expansion can then be implemented separately and repeated for n times, as shown in Fig. 2, which will be discussed in detail in the following subsection.

In the experiment, the number of expansion steps n is finite, which causes a systematic error in this approach. Taking into account n steps, the error after the time t is $\varepsilon = t^3/n^2$ for the second order expansion.[24] For a given time t, this systematic error can be reduced through improving the number of expansion steps. The precision of this realization is discussed in Section 4.

2.2. Diffraction as a free propagator

In non-relativistic quantum mechanics, the time evolution of a system is depicted by the Schrödinger equation, whose fundamental solution can be given through Green's function, also known as the propagator.[25] For a system with a Hamiltonian H, the propagator can be written as

$$K(x,t;x',t') = \langle x|\hat{U}(t,t')|x'\rangle, \tag{5}$$

where $\hat{U}(t,t')$ represents the time evolution operator from time t' to t and x (x') denotes the general coordinates. The term of kinetic energy in the time evolution operator is known as the propagator of free particle, which in 1D is

$$K(x,t;x',0) = \sqrt{\frac{1}{2\pi \mathrm{i}t}}\exp\left[\mathrm{i}\frac{(x-x')^2}{2t}\right]. \tag{6}$$

For simplicity, we choose natural units $\hbar = m = 1$. Consequently, the time evolution operator of a free particle ($\mathcal{V} = 0$) can be implemented via the propagator in Eq. (6). Here, we show that the small angle diffraction (propagation) of light in free space actually has the same form as the evolution of a free particle.

In optics, the propagation of light follows the Huygens–Fresnel principle, which is stated as

$$E(x,y,z) = \frac{z}{\mathrm{i}\lambda}\iint E(x',y',0)\frac{\mathrm{e}^{\mathrm{i}kr}}{r^2}\mathrm{d}x'\mathrm{d}y'. \tag{7}$$

In a more simple and usable expression, equation (7) can be approximated by the Fresnel diffraction integral, which in 1D scenario reads

$$E(x,z) = \int F(x,z;x',0)E(x',0)\mathrm{d}x', \tag{8}$$

where

$$F(x,z;x',0) = \exp(\mathrm{i}kz)\sqrt{\frac{k}{2\pi \mathrm{i}z}}\exp\left[\mathrm{i}\frac{k(x-x')^2}{2z}\right]. \tag{9}$$

If we let $z/k = t$, according to the de Broglie's relation $p = k$ in Eq. (9), the propagator $F(x,z;x',0)$ in Fresnel diffraction takes exactly the same form as the free propagator in quantum mechanics except for a global phase term.

To derive the Fresnel diffraction formula Eq. (8), we need to apply the paraxial approximation ($r \approx z$) to Eq. (7) and then replace the spherical secondary wavelets with parabolic ones, which is known as the Fresnel approximation ($r \approx z + (x-x')^2/2z$). In the range of a small angle diffraction, i.e., $\rho^2/z^2 \ll 1$ with ρ denoting the characteristic size of the light spot, the Fresnel approximation is equivalent to the paraxial approximation.[26] Therefore, the kinetic term in the time evolution operator $\hat{U}^{(i)}(t)$ can be simulated through the small angles diffraction of light in free space.

2.3. Phase plate as a delta-kick potential

Another term in the Suzuki–Trotter expansion of the time evolution operator is the potential, which will result in a pure phase shift $\exp[-\mathrm{i}V(x)\Delta t]$ to the wave function after an evolution time Δt. Current technologies in adaptive optics can control the wave front arbitrarily with the phase plate or the spatial light modulator (a programmable version of the former).[27] The phase plate can adjust the phase of the light wave front depending on the spatial position without changing its intensity distribution, which is equivalent to multiplying the wave function $\psi(x)$ with a position dependent phase term, i.e., $\exp[-\mathrm{i}\phi(x)]\psi(x)$.

In fact, the phase plate provides an implementation for the time evolution with a delta-kick potential, where a time independent potential $\phi(x)$ appears suddenly in one moment and then immediately disappears. The Hamiltonian for a system with the delta-kick potential takes the form

$$-\frac{1}{2}\frac{\partial^2}{\partial x^2} + \phi(x)\delta(t), \tag{10}$$

where $\delta(t)$ is the Dirac delta function. The corresponding time evolution operator takes the form of a pure phase shift $\hat{U} = \exp[-\mathrm{i}\phi(x)]$. If we set $\phi(x) = V(x)\Delta t$, a phase plate can realize the potential term in the Suzuki–Trotter expansion (Eq. (4)), create a phase shift to the wave function. Here, the "delta-kick" means the interaction time for the phase plate should be very short, so that the diffraction inside the phase plate can be ignored (the phase plate should be as thin as possible). In a simple word, the whole time evolution operator $\hat{U}^{(i)}(t)$ can be simulated approximately with an array composed of a free space diffraction (zero potential), a phase plate (delta-kick potential), and another free space diffraction in order, as shown in Fig. 2.

In the scheme proposed by Lahrz *et al.*, the time evolution operator in atom systems is realized by creating the potential with detuned Gaussian beams which are rich in creating both p- and s-barrier. In this way, the form of the potential is restricted to be Gaussian-like. Our scheme, in contrast, can realize time evolution operators in any type of potentials. If we

want to use another form of potential, we just need to change the phase modulation in the phase plate.

2.4. Interferometer approach for non-unitary operator

In this section, we discuss the realization of another important operator in the supersymmetric relationship, i.e., $\hat{B}^\dagger = [-\partial_x + W(x)]/\sqrt{2}$. In the scheme of Lahrz *et al.*, they proposed to realize $\hat{B}+\hat{B}^\dagger$ instead of $\hat{B}^\dagger$. The former can be approximated via the time evolution operator of a shaking process with a harmonic potential. In their first implementation of $\hat{B}^\dagger$, the initial state is set to be a ground state, as a result, $\hat{B}+\hat{B}^\dagger$ degenerates to $\hat{B}^\dagger$. However, the second $\hat{B}^\dagger$ should be applied to a general state, $\hat{U}^{(1)}(t)\psi_i$, where the term of $\hat{B}$ will not degenerate. The simulation procedure can only reach a fidelity of $1/\sqrt{2}$. Here we show that $\hat{B}^\dagger$ can be implemented with high fidelity in our setup.

As shown in Fig. 3, we propose to implement $\hat{B}^\dagger$ via a Mach–Zehnder interferometer, one arm for the term ∂_x and the other for $W(x)$. As $\hat{B}^\dagger$ is non-unitary, non-unitary elements should be included, e.g., the position dependent intensity modulators. In optics, the lens can perform a Fourier transform to the wave front, that is to say, the wave function in momentum space can be modulated by the lens and amplitude modulators. In the lower arm of the interferometer, we adopt a $4f$ system to realize the term in $\hat{B}^\dagger$ involving the momentum. We insert an intensity modulator $\mathcal{A}(x) = \alpha' kx/f$ at the focal point of the $4f$ system, where α' is a parameter to ensure $|\alpha' kx/f| < 1$ and f is the focal length of the lens. Minus $\mathcal{A}(x)$ means an additional π phase should be added. After performing a parity inversion by using another lens with the same focal length, the wave function in this arm is changed to $-\partial_x\psi_i$ with multiplying a constant factor α'. In the upper arm, for compensating the total length and avoiding the diffraction at this stage, we adopt two lenses to perform parity inversion and insert an intensity modulator $A(x) = \alpha W(-x)$ in the middle of the two lenses (as shown in Fig. 3). The α is a constant for renormalization and minus $A(x)$ means an additional π phase should be added.

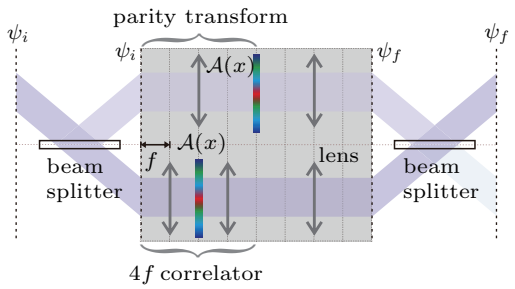


Fig. 3. Mach–Zehnder interferometer with intensity modulator for implementing the non-Hermitian operator $\hat{B}^\dagger$. In the upper arm, two lenses acting as parity transforms are employed for light propagation without diffraction. A position dependent intensity modulator is inserted for implementing the term $\alpha W(x)$ in the operator. In the lower arm, we firstly adopt a $4f$ system with an intensity modulator inserted in the second focal point for simulating the operation in momentum space. Then we perform a parity transform with another lens. Combination of the two arms can give the target wave function.

The final wave function in this arm reads $\alpha W(x)\psi_i$. Finally, the combination of the two arms can give the complete realization of $\hat{B}^\dagger$ by setting $\alpha = \alpha'$. Our approach to the non-unitary operator $\hat{B}^\dagger$ can reach high fidelity, which is shown in the following numerical simulations.

3. Numerically simulated results

As stated in the previous section, our scheme can be applied to any type of superpotential by adjusting the phase modulation of the phase plate. The initial state can also be prepared in any form with wave front modulators. Here, for the sake of better understanding, we consider the same scenario as reported in Ref. [17], where the superpotential reads

$$W(x) = \sqrt{\omega}\{x/x_0 + A\exp[-x^2/(4\sigma^2)]\}. \tag{11}$$

Thus the potentials $V^{(1)}(x)$ and $V^{(2)}(x)$ in the supersymmetric partner Hamiltonians take the form

$$V^{(i)}(x) = \frac{\omega^2 x^2}{2} \mp \frac{\omega}{2} + \frac{\omega A^2}{2}\exp\left(-\frac{x^2}{2\sigma^2}\right) \times \frac{2\omega A x}{x_0}\left(1 \mp \frac{x_0^2}{4\sigma^2}\right)\exp\left(-\frac{x^2}{4\sigma^2}\right), \tag{12}$$

which contains two terms, the harmonic potential $V_{\rm osc} = \omega^2 x^2/2$ and the additional potential $V_{\rm loc}^{(i)}$. The parameter A is set to $\sqrt{26}$. In the potential $V_{\rm osc}$, ω is the trap frequency and $x_0 = \sqrt{1/\omega}$ stands for the harmonic oscillator length. The term of additional potential acts as the barrier, which falls off on a length scale $\sigma = x_0/2$. The structures of energy level for the two potentials are plotted in Fig. 4, where the supersymmetric relationship is shown clearly.

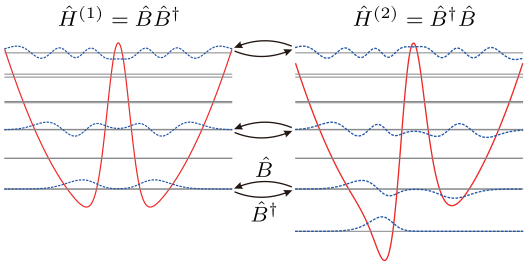


Fig. 4. Supersymmetric potentials (red solid lines) and their energy levels (black solid lines). We can clearly see that the spectra of the two potentials coincide with only an exception of the ground state (unbroken symmetry). The wave packet split into two packets during the evolution because of the existence of the barrier.

For optical simulation, it is more convenient to take the natural length and energy scales, where the energy is measured in units of ω and the distance is measured in units of its characteristic length x_0. The system is initialized to be a shifted Gaussian wave function $\psi(0) = (\pi x_0^2)^{-1/4}\exp[-(x-5x_0)^2/(2x_0^2)]$. For optical simulation, we choose the photon's wavelength $\lambda = 532\,\text{nm}$ and the characteristic length $x_0 = 1\,\text{mm}$. The evolution time of a single step in the Suzuki–Trotter expansion is set to $\Delta t = T/60$ with $T =$

$2\pi/\omega$ standing for the period, which results in a corresponding propagation distance $z = 1.237$ m for diffraction between the phase plates. Through simulating the experiment we plot the normalized probability densities of the final wave functions $\psi_f^{(1)}(t) = \hat{B}^\dagger \hat{U}^{(1)}(t)\psi(0)$ and $\psi_f^{(2)}(t) = \hat{U}^{(2)}(t)\hat{B}^\dagger\psi(0)$ with t ranging from 0 to $t_r = 3T$ in Figs. 5(a) and 5(b). In Fig. 5(c), we show the deviation between the two wave functions, i.e., the probability intensity of $|\psi_f^{(1)}(t) - \psi_f^{(2)}(t)|^2$. It is obvious that the deviation is relatively small (10^{-3}), indicating the existence of supersymmetry.

For further clarification, we show the probability density distributions at different stages during the time evolution in Figs. 5(d)–5(f). The initial density distributions $|\psi(0)|^2$ and $|\hat{B}^\dagger\psi(0)|^2$ are depicted in Fig. 5(d). $\psi(0)$ is a shifted ground state with its center at $-5x_0$. In Fig. 5(e), we show the probability distributions of the two states inside the two arms before the second $\hat{B}^\dagger$ is applied, which are divergent clearly. After performing the second $\hat{B}^\dagger$ to the state $\hat{U}^{(1)}(t_r)\psi(0)$ in the upper arm, the two final states match each other very well, which can be seen clearly from their probability distributions shown in Fig. 5(f). We have also estimated the fidelity between these two states, which reads 0.9973. The perfect overlap of these two final states clearly shows the existence of supersymmetry again.

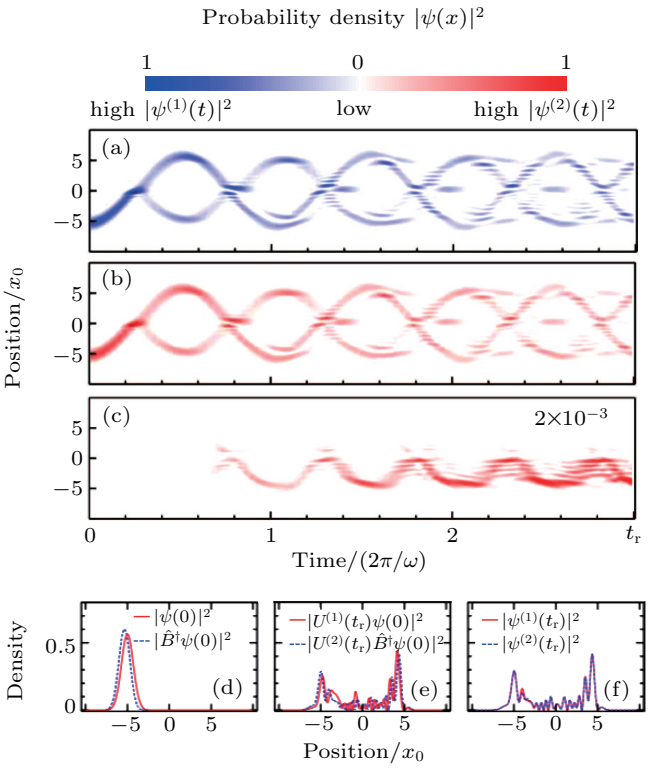


Fig. 5. The normalized probability densities are plotted in (a) for $|\psi_f^{(1)}(t)|^2$ and in (b) for $|\psi_f^{(2)}(t)|^2$. (c) The interference pattern between the two paths $|\psi_f^{(1)}(t) - \psi_f^{(2)}(t)|^2$. (d), (e) The normalized probability densities of $|\psi(0)|^2$ and $|\hat{B}^\dagger\psi(0)|^2$ (d) before the time evolution and (e) at time $t_r = 3T$. In (f), the probability density of the upper path after performing the second $\hat{B}^\dagger$ operation coincides with the lower path very well, which indicates the existence of supersymmetry.

The family of potentials characterized in Ref. [17] for further comparison is as follows:

$$V_\eta(x) = V_{\rm osc}(x) + \frac{\omega A^2}{2}\exp\left(-\frac{2x^2}{x_0^2}\right) + \frac{2\eta\omega A x}{x_0}\exp\left(-\frac{x^2}{x_0^2}\right), \tag{13}$$

which is parameterized by η. The previous potentials then correspond to two special cases $\eta = 0$ for $V^{(1)}(x)$ and $\eta = 1$ for $V^{(2)}(x)$ with neglecting the constant term. As discussed in the previous section, a high fidelity (up to 1) between the final wave functions involving in the evolution governed by the potentials with $\eta = 1$ and $\eta = 0$ can identify the existence of supersymmetry. We depict the numerically simulated fidelity between $\hat{B}^\dagger\hat{U}^{(1)}(t)\psi(0)$ and $\hat{U}_\eta(t)\hat{B}^\dagger\psi(0)$ varying with time and η in Fig. 6(a). In Fig. 6(b), we show the fidelity at time t_r varying with η. We can see that for any evolution time, the fidelity peaks to 1 when $\eta = \pm1$, which clearly shows the existence of supersymmetry ($V_{\eta=-1}(x)$ is also a superpartner potential of $V_{\eta=0}(x)$).

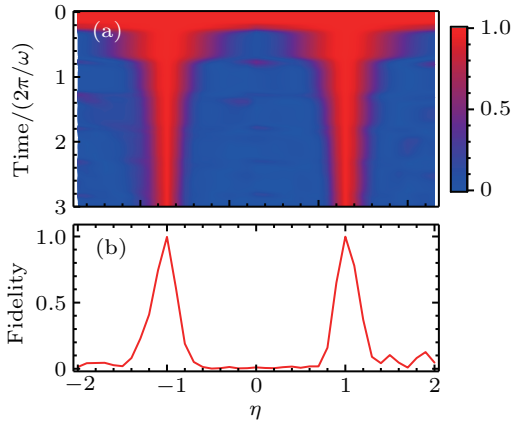


Fig. 6. (a) The fidelity between $\hat{B}^\dagger\hat{U}^{(1)}(t)\psi(0)$ and $\hat{U}_\eta(t)\hat{B}^\dagger\psi(0)$ with t ranging from 0 to $3T$. (b) The fidelity at $t_r = 3T$. The peak-points at $\eta = \pm1$ demonstrate the existence of supersymmetry.

Our scheme is based on an approximate method, i.e., the Suzuki–Trotter expansion. The separated terms in the expansion can be implemented with high fidelity using current available optical elements. So it is necessary to estimate the fidelity of the time evolution operator. Higher order approximation in Suzuki–Trotter expansion can provide higher operation fidelity, which is also more difficult to realize in the experiment. Here we adopt the second order approximation, which is easy to realize and can provide enough operation fidelity. Considering the time evolution of the second subsystem, i.e., the time evolution along the lower arm, the initial state is $\hat{B}^\dagger\psi(0)$ and the final state after half a period of evolution, i.e., at time $T/2$ can be calculated by performing an operator $\hat{U}^{(2)}(T/2)$ on the initial state. We need to repeat the calculation 30 cycles for the single step time evolution ($\Delta t = T/60$) to get the final state at $T/2$. We depict its amplitude and phase by blue solid lines in

Fig. 7(a) with the exact results from the solution of the system's Schrödinger equation shown by red dashed lines. It is clearly shown that the simulated and exact results are in good agreement except for the region where the probability is lower than 10^{-6}. We compare the simulated and exact final states quantitatively by the fidelity, which reads 0.9998 for this time scale. This fidelity can also be improved via increasing the number of steps, i.e., dividing the time into shorter time slices, which requires shortening the diffraction length, provided the condition for the Fresnel approximation is fulfilled. In our simulation, the characteristic size of the light spot is around $10x_0$, therefore the condition of small angles of diffraction is fulfilled in our scenario ($\sim 10^{-4}$). In our consideration, the small angles approximation is completely fulfilled, as the total spot size is $\rho \sim 10$ mm and the diffraction length $z \sim 10^3$ mm, then $\rho^2/z^2 \sim 10^{-4} \ll 1$. Additionally, we can squarely reduce the system size z via reducing the characteristic length x_0 according to the constraints $z = 2\pi N x_0^2/\lambda$ (N stands for the time interval Δt in units of $1/\omega$). The paraxial condition should be fulfilled after reducing the system size.

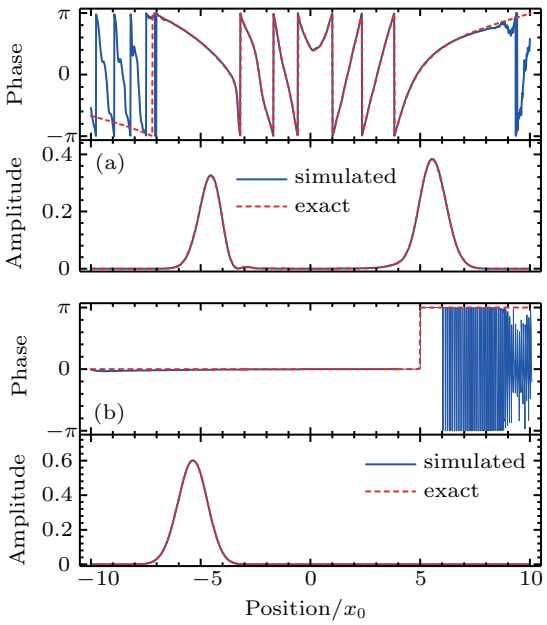


Fig. 7. In (a), we set the initial state to $\hat{B}^\dagger\psi(0)$ and compare the final states $\hat{U}^{(2)}(T/2)\hat{B}^\dagger\psi(0)$ which are calculated through solving the Schrödinger equation (red dashed line) and simulating the experimental scheme (blue solid line). In (b), we show the final states $\hat{B}^\dagger\psi(0)$ which are obtained through algebraic calculation and simulation of the experimental scheme. In both (a) and (b), the two wave functions overlap very well except some low-probability regions $< 10^{-6}$ because of the numerical precision, where the phases diverse the exact values. In (a), the fidelity of the two states reaches 0.99976. In (b), the error rate is lower than 10^{-5}.

Further, we estimate the fidelity in case of non-unitary $\hat{B}^\dagger$ for our current setup. In the numerical simulation, we take the lens as ideal and its effect is like a position dependent phase gate on the wave front, that is multiplying $\exp[-ikx^2/(2f)]$ to the wave function in the clear aperture $x \in [-10x_0, 10x_0]$. The focal length of the lens is set to $f = 0.8$ m. In Fig. 7(b), we show both the amplitude and phase of the final state after acting the operator $\hat{B}^\dagger$ on the initial state $\psi(0)$. It is clearly shown that our scheme can provide high fidelity (error rate lower than 10^{-5}) for implementing $\hat{B}^\dagger$. Our method needs the paraxial condition $f^2/\rho^2 \gg 1$ which equals 6.4×10^3 in our numerical simulation. The further simulation shows that the error rate can be lower than 10^{-3} if it is bigger than 2.5×10^3. Additionally, we need to emphasize that our approach to $\hat{B}^\dagger$ is independent of the initial state.

4. Discussion and conclusion

In this paper, we propose to extend the interferometer scheme for detecting the supersymmetric dynamics in Ref. [17] into linear optics. It is shown in numerically simulated results that our protocol provides good remarks of the supersymmetric dynamics of the superpartner via the destructive interference. The full wave function of a single photon can be directly measured through a technology recently developed from the concept of weak measurement and weak value.[28] It is important to note that the interferometer approach is not necessary for our scheme. Both the final wave functions along the up and bottom arms can be fully reconstructed and then the supersymmetric relationship can be verified directly via calculating the fidelity between these two final wave functions. Such an alternative method can avoid the challenge of stabilizing the interferometer and provide more feasible for experiment with current technologies. Besides, while our work shows the supersymmetric dynamics via the interference between two paths for a given initial state, the implementation of the time evolution operator is based on the Hamiltonian and is independent of the initial state.

References

[1] Dine M 2016 *Supersymmetry and string theory: Beyond the standard model* (Cambridge: Cambridge University Press)
[2] Kane G L and Shifman M A 2001 *The supersymmetric world: the beginnings of the theory* (Singapore: World Scientific)
[3] Weinberg S 2005 *The Quantum Theory of Fields: Volume 3, Supersymmetry* (Cambridge: Cambridge University Press)
[4] Grodon K 2010 *Perspectives On Supersymmetry II* (Singapore: World Scientific)
[5] Nath P 2016 *Supersymmetry, Supergravity, and Unification* (Cambridge: Cambridge University Press)
[6] Binétruy P 2012 *Supersymmetry: Theory, Experiment, and Cosmology* (Oxford: OUP Oxford)
[7] Witten E 1981 *Nucl. Phys. B* **188** 513
[8] Sukumar C V 1985 *J. Phys. A: Math. Gen.* **18** 2917
[9] Cooper F, Khare A and Sukhatme U 1995 *Phys. Rep.* **251** 267
[10] Gangopadhyaya A, Mallow J V and Rasinariu C 2011 *Supersymmetric Quantum Mechanics: An Introduction* (Singapore: World Scientific)
[11] Haber H E and Haskins L S 2018 *Anticipating the Next Discoveries in Particle Physics* (Singapore: World Scientific) pp. 355–499
[12] Ovchinnikov I V and Enßlin T A 2016 *Phys. Rev. D* **93** 085023

[13] Efetov K 1999 *Supersymmetry in disorder and chaos* (Cambridge: Cambridge University Press)
[14] Miri M, Heinrich M, El-Ganainy R and Christodoulides D N 2013 *Phys. Rev. Lett.* **110** 233902
[15] Miri M, Heinrich M and Christodoulides D N 2014 *Optica* **1** 89
[16] Heinrich M, Miri M, Stützer S, El-Ganainy R, Nolte S, Szameit A and Christodoulides D N 2014 *Nat. Commun.* **5** 3698
[17] Lahrz M, Weitenberg C and Mathey L 2017 *Phys. Rev. A* **96** 043624
[18] Aspuru-Guzik A and Walther P 2012 *Nat. Phys.* **8** 285
[19] Georgescu I M, Ashhab S and Nori F 2014 *Rev. Mod. Phys.* **86** 153
[20] Makri N and Miller W H 1989 *J. Chem. Phys.* **90** 904
[21] Zagury N, Aragão A, Casanova J and Solano E 2010 *Phys. Rev. A* **82** 042110
[22] Argeri M, Di Vita S, Mastrolia P, Mirabella E, Schlenk J, Schubert U and Tancredi L 2010 *J. High Energy Phys.* **2014** 82
[23] Suzuki M 1976 *Comm. Math. Phys.* **51** 183
[24] Dhand I and Sanders B C 2014 *J. Phys. A: Math. Gen.* **47** 265206
[25] Sakurai J J and Napolitano J 2011 *Modern quantum mechanics* (2nd Edn.) (Boston: Addison-Wesley)
[26] Goodman J W 2017 *Introduction to Fourier optics* (4nd Edn.) (New York: W. H. Freeman, Macmillan Learning)
[27] Tyson R K 2015 *Principles of Adaptive Optics* (4nd Edn.) (New York: CRC Press)
[28] Lundeen J S, Sutherland B, Patel A, Stewart C and Bamber C 2011 *Nature* **474** 188